



A Phase Sensitivity-Enhanced Surface Plasmon Resonance Biosensor Based on ITO-Graphene Hybrid Structure

Lei Han¹ · Chuan Wu¹

Received: 6 August 2018 / Accepted: 5 November 2018 / Published online: 28 November 2018
© Springer Science+Business Media, LLC, part of Springer Nature 2018

Abstract

In this paper, a surface plasmon resonance (SPR) sensor based on the hybrid structure of silver (Ag)-indium tin oxide (ITO)-graphene is proposed and investigated. SPR biosensors are subdivided into three kinds of structures Ag, Ag-graphene, and Ag-ITO-graphene, when carried out using their respective optimized structure parameters. According to our analysis and comparison, the ITO-assisted SPR biosensor has an optimal reflectivity of 3.587×10^{-8} and a maximum phase sensitivity of $1.707 \times 10^{6\circ}/\text{RIU}$, which shows that ITO can be employed to further enhance the SPR sensing performance even with the existence of graphene.

Keywords Surface-plasmon-resonance · Phase sensitivity · Reflectivity · Hybrid structure

Introduction

Surface plasmons (SPs) are electronic dilatational waves transmitting on a metal surface that are generated by the interaction between freely vibrating electrons and photons existing on that metal surface. A feature of the propagation of SP waves is that they are highly sensitive to the variation of refractive index of the dielectric adjacent to the metal. The most conventional approach to stimulating the excitation of surface plasmon is the Kretschmann configuration, in which a prism is coupled with a thin metal film [1]. SPR is greatly applied in biological science, gas detection, and environmental monitoring thanks to its many advantages such as smaller size, low-cost components, highly controllable, multiple channels and better reflectivity and sensitivity [2]. In order to improve the sensitivity of these kinds of sensors, over the past decade, many researchers have investigated SPR in aspects of, for example, improving the materials [3–5], changing the geometrical shapes [6, 7], or increasing the number of the channels [8, 9].

It is well known that graphene can be used to improve the sensitivity of conventional SPR structure. Graphene is a two-

dimensional carbon material which has favorable strength, malleability, electrical conductivity, thermal conductivity, and optical properties and therefore, has been widely applied in biological science, electronic information, and aerospace [10–12]. There are several advantages for using graphene-based SPR substrate for sensing. First, they can induce large field enhancement at the substrate interface. Second, graphene has a large surface area, which makes it have better surface contact. Finally, graphene surface specific detection of aromatic compounds via polyimide (PI) layer force, which will help challenge experimental studies and other interactions with protein DNA in extremely dilute conditions [13–15]. The SPR sensor based on graphene-on-metal has also been researched in order to improve the sensing performance [16].

On the other hand, the transparent conductive ITO has also attracted great attention since it can be used as the functional material for modulators and SPR with the advantages of tunable permittivity, low capacitance, and high transmittance [17–21]. The transparency of ITO film can be as high as 95% for visible lights and 80% for infrared lights. As proven by Byun K M et al., ITO is able to enhance SPR's sensitivity in the visible range [17]. Gupta B D et al. utilized ITO to prepare SPR ammonia gas and PH sensors, and demonstrated that the sensitivity and the operating range of the sensor is highly depended on ITO's thickness [18, 19]. A. K. Mishra et al. designed a highly sensitive SPR sensor working in the infrared band and proved that ITO offers a positive effect on enhancing SPR's sensitivity [20].

✉ Lei Han
hanlei@cug.edu.cn

¹ School of Mechanical Engineering and Electronic Information, China University of Geosciences (Wuhan), Wuhan 430074, China

It should be noted that most of the previous sensor designs focus on angular or intensity interrogation. However, angular interrogation requires high precision instruments to track the variation of the resonance angle, which is not that cost-effective while the intensity noise of light source can significantly limit the achievable low detection limit of the intensity-interrogation-based sensor. Such a drawback can be gained by passing from angular/intensity interrogation to phase interrogation [22–24], since generally phase noises of laser sources are orders of magnitude lower compared to the intensity ones. In phase interrogation, the p-polarized “probe” beam and s-polarized “reference” beam experience different phase shift; the differential phase shift thus can be employed as a sensing parameter.

As mentioned above, though both graphene and ITO have been proven to possess the capability of sensitivity enhancement, how the performances can be affected by combining these two materials in a single SPR sensor has not been revealed, especially their impacts on phase sensitivity. In this paper, we propose a SPR biosensor with Ag-ITO-graphene hybrid structure and investigate its reflectivity and phase sensitivity at visible wavelength. It is found that ITO and graphene can be combined to further enhance the sensitivity.

Sensor Configuration and Investigation Method

In the proposed SPR sensor, the Kretschmann configuration is considered, in which a thin Ag film coated with glass slide is attached to the base of an equilateral prism made of high refractive index glass through an index matching fluid. The SPR sensor with Ag-ITO-graphene structure is shown in Fig. 1. This structure contains seven layers, namely Prism, BK7 glass slide, Ag, ITO, graphene, and analyte, among which BK7 and Ag are bind together via the titanium adhesion

layer. The He-Ne laser of wavelength 632.8 nm is fixed as p-polarized light.

The first layer is the SF11 glass prism and its refractive index (n_1) is calculated through the following relation [25]:

$$n_1 = \sqrt{\frac{1.73759695\lambda^2}{\lambda^2 - 0.013188707} + \frac{0.313747346\lambda^2}{\lambda^2 - 0.0623068142} + \frac{1.89878101\lambda^2}{\lambda^2 - 155.23629} + 1} \quad (1)$$

where λ is the wavelength of incident light. The second layer is the BK7 glass slide and its refractive index (n_2) is determined by the following relation [26]:

$$n_2 = \sqrt{\frac{1.03961212\lambda^2}{\lambda^2 - 0.00600069867} + \frac{0.231792344\lambda^2}{\lambda^2 - 0.0200179144} + \frac{1.01046945\lambda^2}{\lambda^2 - 103.560653} + 1} \quad (2)$$

The complex refractive index of the titanium adhesion layer (n_3) at 632.8 nm is obtained from the experimental measurement data by Palik [25]. The fourth layer is the Ag thin film and its complex refractive index (n_4) is calculated through the Drude dispersive model [27, 28].

$$n_3 = \sqrt{1 - \frac{\gamma_1 \lambda^2}{\gamma_2^2 (\gamma_1 + i\lambda)}} \quad (3)$$

where $\gamma_2 = 0.14541 \mu\text{m}$ is the wavelength corresponding to the bulk plasma frequency and $\gamma_1 = 17.6140 \mu\text{m}$ denotes the collision wavelength and is related to the losses.

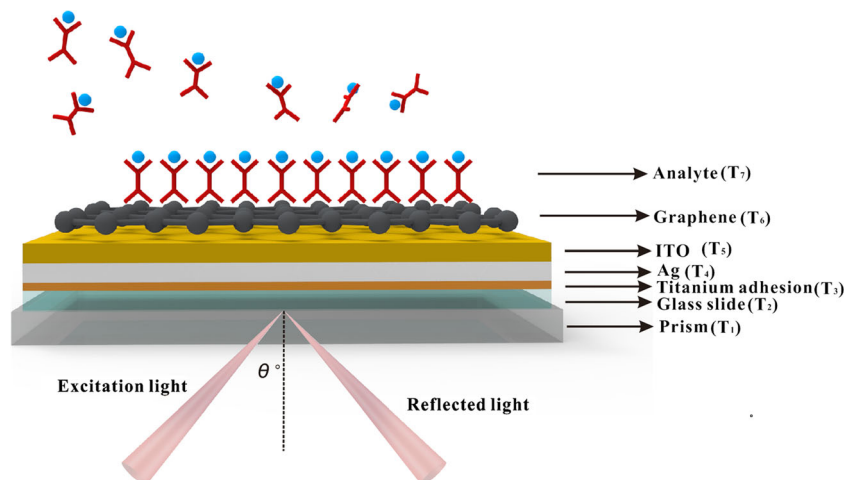
The fifth layer of ITO film’s optical properties can be quantitatively described by using the classical Drude free-electron theory [29].

$$n_5 = \sqrt{3.8 - \frac{\gamma_c \lambda^2}{\gamma_p^2 (\gamma_c + i\lambda)}} \quad (4)$$

where the $\gamma_p = 0.56497 \mu\text{m}$ and $\gamma_c = 11.21076 \mu\text{m}$.

The seventh layer of model is graphene and its complex refractive index (n_6) in the visible range is given as [30]

Fig. 1 Schematic diagram of the proposed SPR biosensor with Ag-ITO-graphene hybrid structure



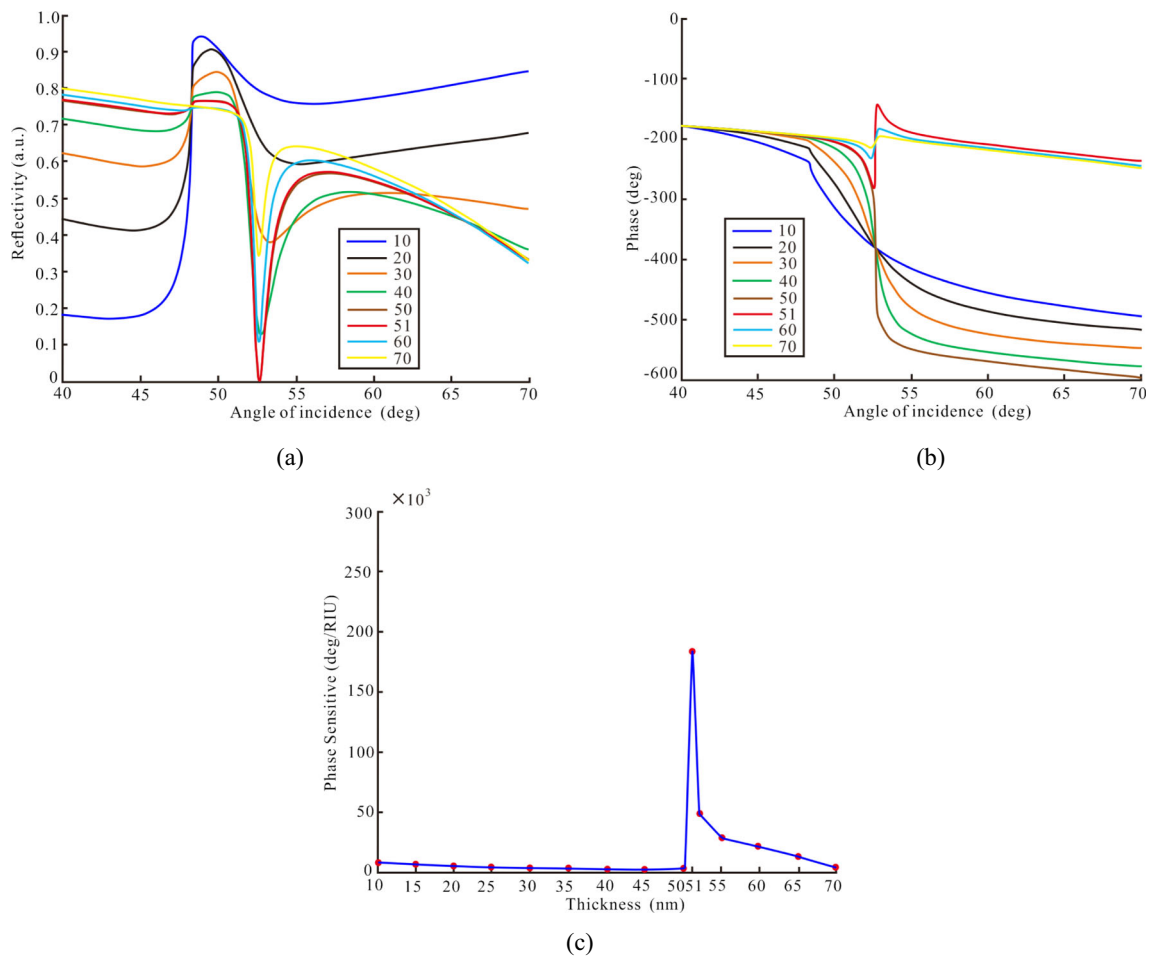


Fig. 2 Variation of **a** reflectivity and **b** phase with respect to angle of incidence, **c** phase sensitive with respect to Ag thickness (nm)

$$n_6 = 3.0 + i\frac{C_1}{3}\lambda \tag{4}$$

where the constant $C_1 \approx 5.446 \mu\text{m}^{-1}$ is implied by the opacity measurement by Nair [31]. The thickness of monolayer graphene is 0.34 nm. The sensing medium for initial calibration is deionized (DI) water and its refractive index (n_7) is 1.333 [32]. The refractive index change of the sensing medium induced by the adsorption of biomolecules on the surface of monolayer graphene is denoted by Δn_{bio} . Thus, based on the above parameters and equations, the refractive indices of the seven layers used in our SPR modeling at 632.8 nm are respectively: $n_1 = 1.7786$, $n_2 = 1.5151$, $n_3 = 2.1526 + i3 \times 2.9241$, $n_4 = 0.1350 + i4 \times 3.9850$, $n_5 = 1.8580 + i5 \times 0.0580$, $n_6 = 3 + i6 \times 1.1487$, $n_7 = 1.3330 + \Delta n_{\text{bio}}$.

In order to investigate the sensing performance, we have applied the transfer matrix method (TMM) and Fresnel equations based on an N-layer model to carry our analysis in details. For each layer, the dielectric constant ($\epsilon = n^2$) and the thickness (d) of the layer are decisive factors, and all layers are optically isotropic and nonmagnetic. In the electromagnetic field, tangential direction of the first boundary Z_1 is $Z =$

$Z_1 = 0$. In consideration to the last boundary Z_{N-1} tangential field, we have the control point of the first boundary Z_1 [29, 30]:

$$\begin{bmatrix} H_1 \\ W_1 \end{bmatrix} = M \begin{bmatrix} H_{N-1} \\ W_{N-1} \end{bmatrix} \tag{5}$$

where H_1 and H_2 are tangential components of the first and the n th layer of the electric field, respectively; W_1 and W_{N-1} are tangential components of the first and the n th layer of the boundary magnetic field, respectively; and M represents the combination of the layer structure of the transfer matrix (TM). The interference matrix of the N-layer structure can be expressed by

$$M = \prod_{k=2}^{N-1} M_k = \begin{bmatrix} M_{11} & M_{12} \\ M_{21} & M_{22} \end{bmatrix} \tag{6}$$

where M_k is expressed as

$$M_k = \begin{bmatrix} \cos\alpha_k & (-i\sin\alpha_k)/p_k \\ -ip_k\sin\alpha_k & \cos\alpha_k \end{bmatrix} \tag{7}$$

where P_k and α_k are written as

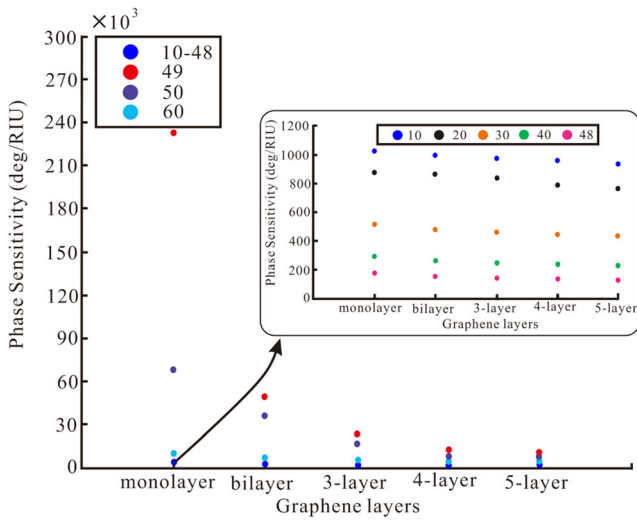


Fig. 3 Variation phase sensitivity for diverse layers of graphene and different thickness of Ag (nm)

$$p_k = \sqrt{\left(\frac{\nu_k}{\varepsilon_k}\right) \cos\theta_k} = \frac{\sqrt{\varepsilon_k - n_1^2 \sin^2\theta_1}}{\varepsilon_k} \quad (8)$$

$$\alpha_k = \frac{2\pi d_k}{\lambda} \sqrt{\varepsilon_k - n_1^2 \sin^2\theta_1} \quad (9)$$

where ε_k and d_k are the dielectric constant and the thickness of the k th layer, respectively, and θ_1 and λ are incident angle and wavelength, as shown in Fig. 1. The matrix of the total reflection polarized light (γ_p) can be expressed as

$$\gamma_p = \frac{(M_{11} + M_{12}p_N)p_1 - (M_{21} + M_{22}p_N)}{(M_{11} + M_{12}p_N)p_1 + (M_{21} + M_{22}p_N)} \quad (10)$$

where p_1 represents the relation between the prism (at the first layer) and the dielectric constant and p_N represents the relation between the analyte (at the n th layer) and the dielectric

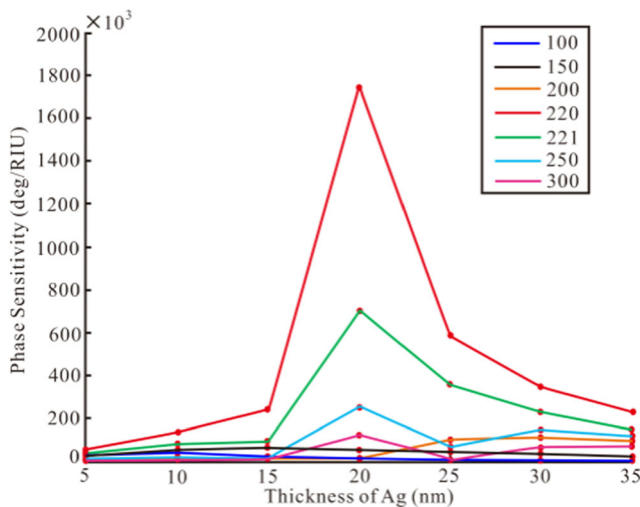


Fig. 4 Variation phase sensitivity for different thicknesses of Ag and ITO (nm)

constant. Finally, the reflectance (R_p) for p-polarized wave is obtained:

$$\phi_p = \arg(\gamma_p) \quad (11)$$

$$R_p = |\gamma_p|^2 \quad (12)$$

The SPR phase sensitivity (S_p) is defined as

$$S_p = \frac{\Delta\phi_p}{\Delta n_{\text{bio}}} \quad (13)$$

In order to highlight the enhancement provided by graphene -ITO hybrid structure, in the following sections, we optimize the SPR sensor with conventional metal-dielectric structure, metal-dielectric-graphene structure, and metal-dielectric-graphene-ITO hybrid structure progressively and compare their sensitivity.

Analysis and Discussion

Metal-Dielectric Structure

In this structure, T_5 (ITO) and T_6 (graphene) layers of the Ag-ITO-graphene hybrid structure are removed, where the T_n represents n th layer. In the following analysis, the thicknesses of the first three layers are fixed at $d_1 = 200$ nm, $d_2 = 100$ nm, and $d_3 = 2.5$ nm, respectively. The sensing medium of water refractive index variation (Δn_{bio}) is 0.0001. We optimize the thicknesses of Ag on SPR's performance, namely the reflectivity and the phase sensitivity. The reflectivity and the phase sensitivity are investigated by changing the thickness of Ag. Figure 2a, b shows the variation of reflectivity and phase with respect to angle of incidence for different thickness of Ag. The phase sensitivity with respect to Ag thickness is shown in

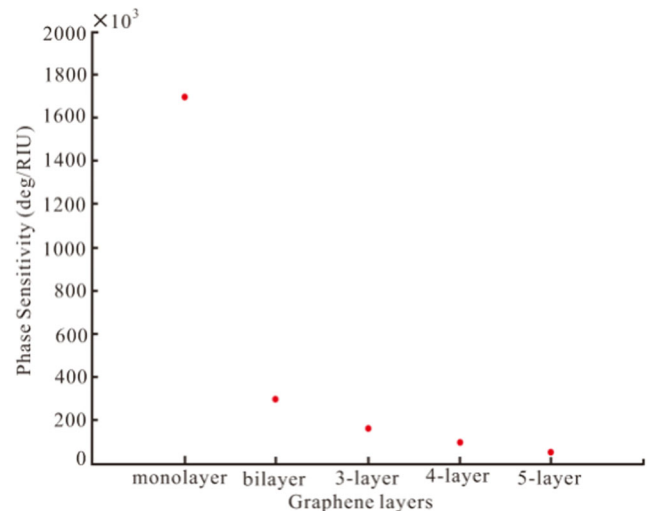


Fig. 5 Variation phase sensitivity for different layers of graphene

Table 1 Three structures sensing performances of reflectivity and phase sensitivity

Multilayer structure	Ag (nm)	ITO (nm)	Graphene (nm)	Reflectivity (a.u.)	Sensitivity ($^{\circ}$ /RIU)
Metal-dielectric	51	0	0	7.759×10^{-4}	1.736×10^5
Metal-graphene-dielectric	49	0	0.34	5.684×10^{-6}	2.358×10^5
Metal-graphene-ITO-dielectric	20	220	0.34	3.587×10^{-8}	1.707×10^6

Fig. 2c. A peak value of $\sim 1.736 \times 10^5$ / $^{\circ}$ RIU can be achieved with Ag thickness of 51 nm.

From Fig. 2a, Ag with different thickness puts up different reflectivity characteristics in SPR with increasing incident angle. When the incident angle is 52.72° , the reflectivity is the optimal value. When the thickness of Ag increases from 10 to 50 nm, the reflectivity decreases from 0.757 to 8.237×10^{-3} a.u. When the thickness of Ag is 51 nm, the reflectivity has touch bottom 7.759×10^{-4} a.u. Nevertheless, when the thickness of Ag increases from 52 to 70 nm, the reflectivity increases from 4.235×10^{-3} to 0.337 a.u. SPR has the characteristics of phase change due to the change of reflectivity [33]. From Fig. 2b, the change of phase reaches the maximum when the thickness of Ag is 51 nm. In the metal-dielectric structure, the thickness of Ag is the best in 51 nm. From Fig. 2c, when the thickness of Ag increases from 10 to 50 nm, the phase sensitivity decreases from 1029.2 to 158° /RIU. When the thickness of Ag is 51 nm, the phase sensitivity reaches 1.736×10^5 / $^{\circ}$ RIU. However, when the thickness of Ag increases from 52 to 70 nm, the phase sensitivity decreases from 4.488×10^4 to 4.309×10^3 / $^{\circ}$ RIU. Therefore, in the metal-dielectric structure, when the thickness of Ag is 51 nm, the phase sensitivity is the highest.

Metal-Graphene Hybrid Structure

Graphene is known as a functional material to enhance the sensing performance. For Ag-graphene structure, T_5 (ITO) is removed and different layers of graphene are added to evaluate their contributions. When the thickness of Ag changes from 10 to 60 nm, the different layers of graphene have diverse peaks. The thickness of graphene of monolayer, bilayer, 3-layer, 4-layer, and 5-layer are 0.34 nm, 0.68 nm, 1.02 nm, 1.36 nm, and 1.70 nm, respectively. When the incident angle is 52.91° , the reflectivity is the optimal value. From Fig. 3, when the thickness of Ag increases from 10 to 48 nm, the phase sensitivity of graphene in the same layer is decreasing. In addition, with the increase of the number of graphene layers, the phase sensitivity is also decreasing. When the graphene is monolayer and the thickness of Ag is 49 nm, a peak value of $\sim 2.358 \times 10^5$ / $^{\circ}$ RIU can be achieved. When the thickness of Ag increases from 50 to 60 nm, the phase sensitivity of graphene in the same layer decreases from 6.879×10^4 to 7.521×10^3 / $^{\circ}$ RIU, and with the increase of the number of graphene layers, the phase sensitivity is getting lower and

lower. Therefore, in metal-graphene hybrid structure, when the thickness of Ag is 49 nm and the graphene is monolayer, the phase sensitivity is the highest.

Metal-Graphene-ITO Hybrid Structure

According to the above analysis, it can be found that though graphene is able to improve the phase sensitivity, the enhancement is not that prominent. For comparison, the Ag-graphene-ITO hybrid structure is investigated. First, the different thickness of Ag and ITO are analyzed when the graphene is monolayer. Figure 4 shows the phase sensitivity for different thickness of Ag and ITO. When the incident angle is 49.45° , the reflectivity is the optimal value. When the thickness of ITO and Ag are 100 and 5 nm, the phase sensitivity is 1.683×10^3 / $^{\circ}$ RIU. With the increase of the thickness of Ag, the phase sensitivity decreases gradually, as far as the thickness of Ag is 35 nm, the phase sensitivity is 386.96° /RIU. When the thickness of ITO and Ag are 150 and 15 nm, the phase sensitivity reaches the highest for 3.526×10^4 / $^{\circ}$ RIU. When the thickness of Ag is 20 nm and the thickness of ITO is 220 nm, the phase sensitivity is maximum of 1.707×10^6 / $^{\circ}$ RIU. When the thickness of ITO and Ag are 221 and 20 nm, the highest of phase sensitivity is obtained by 7.43×10^5 / $^{\circ}$ RIU. When the thickness of ITO is 250 nm and 300 nm, the maximum phase sensitivity of Ag at 30 nm is 2.135×10^4 / $^{\circ}$ RIU and 2.133×10^3 / $^{\circ}$ RIU, respectively. Then, the influence of the number of graphene layers on the resonance spectra is explored. With the increase of graphene layer number, the phase sensitivity is gradually reduced, when the thickness of Ag is 20 nm and the thickness of ITO is 220 nm, which is showed in Fig. 5. Therefore, when the thickness of Ag, graphene, and ITO are 20 nm, monolayer and 220 nm respectively, a peak value of $\sim 1.707 \times 10^6$ / $^{\circ}$ RIU can be achieved.

For comparison, the optimized structure parameters and corresponding sensing performances of the three structures are listed in Table 1.

Conclusion and Discussion

In this paper, three SPR biosensors based on Ag, Ag-graphene, and Ag-ITO-graphene are optimized and compared. The SPR sensor based on Ag-ITO-graphene structure with phase sensitivity of 1.707×10^6 / $^{\circ}$ RIU shows better

performance when compared to the other two. It is therefore reasonable to conclude that ITO can be used to further enhance the performance of SPR biosensor, especially the phase sensitivity. Hence, we believe that the proposed sensor is of a great potential in biomolecule sensing applications.

Funding Information This work was partially supported by the Fundamental Research Funds for National University, China University of Geosciences (Wuhan) (1810491T06).

References

- Patching SG (2014) Surface plasmon resonance spectroscopy for characterisation of membrane protein–ligand interactions and its potential for drug discovery. *Biochim Biophys Acta Biomembr* 1: 43–55
- Shrivastav AM, Gupta BD (2016) SPR and molecular imprinting-based fiber-optic melamine sensor with high sensitivity and low limit of detection. *IEEE J SEL TOP QUANT* 22:172–178
- Zhang J, Chen TP, Li XD, Liu YC, Liu Y, Yang HY (2016) Investigation of localized surface plasmon resonance of TiN nanoparticles in TiN \times O y thin films. *Opt Mat Express* 6(7):2422–2433
- Wang F, Wang M, Li D, and Yang D (2012) Localized surface plasmon resonance enhanced photoluminescence from SiNx with different N/Si ratios. *Opt. Mat. Express* 210:1437–1448
- Martin J, Proust J, Gérard D, Plain J (2013) Localized surface plasmon resonances in the ultraviolet from large scale nanostructured aluminum films. *Opt Mat Express* 3:954–959
- Rifat AA, Mahdiraji GA, Sua YM, Ahmed R, Shee YG, Adikan FM (2016) Highly sensitive multi-core flat fiber surface plasmon resonance refractive index sensor. *Opt Express* 24:2485–2495
- Yuan J, Xie Y, Geng Z, Wang C, Chen H, Kan Q, Chen H (2015) Enhanced sensitivity of gold elliptic nanohole array biosensor with the surface plasmon polaritons coupling. *Opt Mat Express* 5:818–826
- Derenko S, Kullock R, Wu Z, Sarangan A, Schuster C, Eng LM, Härtling T (2013) Local photochemical plasmon mode tuning in metal nanoparticle arrays. *Opt Mat Express* 3:794–805
- Peng L, Shi Fk, Zhou GY, Ge S, Hou Z and Xia C A (2015) Surface plasmon biosensor based on a D-shaped microstructured optical fiber with rectangular lattice, *IEEE Photonics J.* 7(5): 4801309
- Wu J (2016) Tunable ultranarrow spectrum selective absorption in a graphene monolayer at terahertz frequency. *J Phys D Appl Phys* 49: 215108
- Huang L, Wu S, Wang Y, Ma X, Deng H, Wang S, Li T (2017) Tunable unidirectional surface plasmon polariton launcher utilizing a graphene-based single asymmetric nanoantenna. *Opt Mat Express* 7:569–576
- Chiu NF, Huang TY (2014) Sensitivity and kinetic analysis of graphene oxide-based surface plasmon resonance biosensors. *Sensors Actuators B: Chemical* 197:35–42
- Wu L, Chu HS, Koh WS, Li EP (2010) Highly sensitive graphene biosensors based on surface plasmon resonance. *Opt Exp* 18: 14395–14400
- Song B, Li D, Qi WP, Elstner M, Fan CH, Fang HP (2010) Graphene on Au(1 1 1): a highly conductive material with excellent adsorption properties for high-resolution bio/nanodetection and identification. *ChemPhysChem* 11:585–589
- McGaughey GB, Gagne M, Rappe AK (1998) Pi-stacking interactions – alive and well in proteins. *J Biol Chem* 273:15458–15463
- Verma A, Prakash A, Tripathi R (2014) Performance analysis of graphene based surface plasmon resonance biosensors for detection of pseudomonas-like bacteria. *Opt Quant Electron* 47:1197–1205
- Byun KM, Kim NH, Leem JW, Yu JS (2012) Enhanced surface plasmon resonance detection using porous ITO–gold hybrid substrates. *Applied Physics B* 107:803–808
- Mishra SK, Kumari D, Gupta BD (2012) Surface plasmon resonance based fiber optic ammonia gas sensor using ITO and polyaniline. *Sensors Actuators B Chem* 171:976–983
- Mishra SK, Gupta BD (2013) Surface plasmon resonance based fiber optic pH sensor utilizing Ag/ITO/Al/hydrogel layers. *Analyst* 138:2640–2646
- Mishra AK, Mishra SK (2015) Infrared SPR sensitivity enhancement using ITO/TiO2/silicon overlays. *EPL (Europhysics Letters)* 112:10001
- Han L, Ding HF, Huang TY, Wu X, Chen B, Ren K, Fu S (2018) Broadband optical reflection modulator in indium-tin-oxide-filled hybrid plasmonic waveguide with high modulation depth. *Plasmonics* 13(4):1309–1314
- Huang YH, Ho HP, Wu SY, Kong SK, Wong WW, Shum P (2011) Phase sensitive SPR sensor for wide dynamic range detection. *Opt Lett* 36:4092–4094
- Shao Y, Li Y, Gu D, Zhang K, Qu J, He J, Niu H (2013) Wavelength-multiplexing phase-sensitive surface plasmon imaging sensor. *Opt Lett* 38:1370–1372
- Zhang C, Wang R, Min C, Zhu S, Yuan XC (2013) Experimental approach to the microscopic phase-sensitive surface plasmon resonance biosensor. *Appl Phys Lett* 102:011114
- Palik ED (1985) *Handbook of optical constants of solids*. Academic, New York
- Wijaya E, Lenaerts C, Maricot S, Hastanin J, Habraken S, Vilcot JP, Szunerits S (2011) Surface plasmon resonance-based biosensors: from the development of different SPR structures to novel surface functionalization strategies. *Curr Opinion Solid State Mater Sci* 15: 208–224
- Mishra AK, Mishra SK, Gupta BD (2015) SPR based fiber optic sensor for refractive index sensing with enhanced detection accuracy and figure of merit in visible region. *Opt Commun* 344:86–91
- Iga M, Seki A, Watanabe K (2004) Hetero-core structured fiber optic surface plasmon resonance sensor with silver film. *Sens Actuators B-Chem* 101(3):368–372
- Dodge MJ (1984) Refractive properties of magnesium fluoride. *Appl Opt* 23(12):1980–1985
- Roy K, Padmanabhan M, Goswami S, Sai TP, Ramalingam G, Raghavan S, Ghosh A (2013) Graphene-MoS2 hybrid structures for multifunctional photoresponsive memory devices. *Nat Nanotechnol* 8:826–830
- Nair RR, Blake P, Grigorenko AN, Novoselov KS, Booth TJ, Stauber T, Peres NMR, Geim AK (2008) Fine structure constant defines visual transparency of graphene. *Science* 320(5881):1308–1308
- Lee S, Hyung M, Shin HJ, and Choi D (2013) Control of density and LSPR of Au nanoparticles on graphene. *Nanotechnology* 24: 275702
- Saarinen JJ, Peiponen KE, Vartiainen EM (2003) Simulation on wavelength-dependent complex refractive index of liquids obtained by phase retrieval from reflectance dip due to surface plasmon resonance. *Appl Spectrosc* 57(3):288–292